Tectonic Landform and Paleoseismic Activity of the Northernmost Sumatran Fault, Aceh Province, Indonesia

H. Tsutsumi[1], Y. Soeda[2], N. Ismail[3], B. Ali[3], and T. Tabei[4]

[1]Department of Environmental Systems Science, Doshisha University, Japan.

[2]West Japan Engineering Consultants, Inc., Japan.

[3]Department of Physics, Syiah Kuala University, Indonesia.

[4]Department of Global Environment and Disaster Prevention, Kochi University, Japan.

Corresponding author: Hiroyuki Tsutsumi (htsutsum@mail.doshisha.ac.jp)

Key Points:

- We present detailed analyses of tectonic landform and geologic structures of the northernmost Sumatran fault for the first time.
- A paleoseismic trenching revealed that the average recurrence interval of surface-rupturing earthquakes on the Seulimeum segment is 130-210 years.
- The Sumatran fault near Banda Aceh has not ruptured at least in the past 120 years, and the seismic potential of damaging earthquakes is high.

Abstract

The Sumatran fault is an arc-parallel dextral strike-slip fault that accommodates much of the right-lateral component of oblique subduction of the Indian-Australian plate beneath the Sunda plate. The 1900-km-long fault is divided into multiple segments, some of which ruptured the surface during the moderate to large historical earthquakes. The northern Sumatran fault in Aceh Province has not ruptured in the past 120 years and is considered a seismic gap. Since 2012, we have mapped the northern Sumatran fault based on the ALOS (Advanced Land Observing Satellite) PRISM (Panchromatic Remote-sensing Instrument for Stereo Mapping) satellite images. We also conducted several campaigns of geologic fieldworks. The Sumatran fault in the study area is composed of the Aceh and Seulimeum segments. Both segments exhibit conspicuous tectonic landforms, including fault scarps, aligned saddles, offset streams, and linear valleys. The Aceh segment does not show clear geomorphic evidence of late Quaternary movement north of 5°27'N, and the Seulimeum segment appears to accommodate much of the right-lateral motion. We conducted a trenching survey of the Seulimeum segment at Lamtamot, where the fault offsets fluvial terraces. We identified geologic evidence of four surface-rupturing events that occurred after AD1265-1365 and before AD1892. The average recurrence interval of the surface-rupturing earthquake is calculated at 130-210 years. At least 120 years, close to the shortest estimated average recurrence interval, have passed since the last faulting event. We estimate that the probability of a massive earthquake on the northernmost Sumatran fault is high.

1 Introduction

The Sumatran fault in Indonesia is a major trench-parallel strike-slip fault that accommodates a large portion of the right-lateral component of oblique convergence between the Indian-Australian and Sunda plates along the Sunda trench (Fitch, 1972; Yeats, 2012) (Fig. 1). The 1900-km-long fault was first mapped in detail by Sieh and Natawidjaja (2000) based on topographic maps and stereographic aerial photographs. The Sumatran fault is highly segmented and consists of ~20 segments separated by fault trace discontinuities (Sieh and Natawidjaja, 2000; Natawidjaja and Triyoso, 2007). Natawidjaja (2018) compiled and evaluated the published geologic and geodetic slip rates of the fault. He concluded that the right-lateral slip rate is constant at ~15 mm/yr along the length of the fault compared to a previous idea that the slip rate increases northward as the plate convergence obliquity increases to that direction. Hurukawa et al. (2014) mapped the fault planes of M≥7.0 earthquakes along the Sumatran fault since 1892 and identified possible seismic gaps, including the northernmost subaerial segments, the Aceh and Seulimeum segments in Aceh Province.

The 26 December 2004 Sumatra-Andaman earthquake (M_w 9.2) has altered the state of stress in the overriding plate at the Sunda subduction zone. Co-seismic Coulomb stress change for the ~300-km-long section of the northern Sumatran fault is estimated to be a positive loading of up to 0.9 MPa (McCloskey et al., 2005). Ito et al. (2012) deployed a GNSS network across the Sumatran fault in Aceh Province and measured repeatedly since 2005. They documented that the Sumatran fault at a latitude of ~5°N is creeping at a rate of 20 ± 6 mm/yr. Tong et al. (2018) also revealed up to ~20 mm/yr of aseismic creep on the Aceh segment based on the InSAR time series analysis. These geodetic studies clearly illustrate that sizeable elastic strain has been built up in the upper crust along the northernmost Sumatran fault, and its seismic potential is high.

However, geologic data on the northern Sumatran fault are sparse because of the difficulties of geologic fieldwork in the mountainous terrain and unstable political conditions

before the 2004 earthquake. To understand the active tectonics and seismic potential of the northern Sumatran fault in Aceh Province, we have studied the fault based on stereographic satellite images and field investigations, including paleoseismic trenching of the Seulimeum segment, since 2012. In this paper, we describe the tectonic landform and fault structures in detail. We also present geologic evidence of four surface-rupturing earthquakes and the average recurrence interval of large earthquakes on the Seulimeum segment.

2 Methods

To map the surface trace of the Sumatran fault, we interpreted the stereo-pairs of ALOS (Advanced Land Observing Satellite) PRISM (Panchromatic Remote-sensing Instrument for Stereo Mapping) images, which have a surface resolution of 2.5 m. The ALOS had been operated from January 2006 to May 2011 by JAXA (Japan Aerospace Exploration Agency). The PRISM had three independent optical systems to obtain along-track images for forward, nadir, and backward views at the same time (JAXA, 2007), enabling us to utilize stereo-pair images. We acquired nadir- and backward-looking PRISM pair images of northern Sumatra taken between 2007 and 2011, and processed them to make black-and-white 1:30,000-scale stereo images (Fig. 2). One of the drawbacks of the PRISM images is that we can rarely find images without clouds in this tropical area. There were some areas along the fault where we could not analyze tectonic geomorphology due to extensive cloud coverage.

In 2018, the Indonesian Geospatial Information Agency released the DEMNAS (Indonesian Digital Elevation Model) with a spatial resolution of 0.27 arcsecond (~8 m). We prepared stereographic shaded relief maps and interpreted them. We mapped the active faults based on tectonic geomorphic features resulted from repeated faulting in recent geologic time such as linear valleys (depressions), aligned saddles on mountain slopes, stream offsets, fault scarps, and pressure ridges. We utilized the shaded relief maps and 1:50,000-scale topographic maps published by the Indonesian Geospatial Information Agency as base maps for mapping.

Since 2012, we conducted seven campaigns of geologic fieldwork of accessible portions of the fault trace accompanied by recent tectonic geomorphic features. We surveyed from the Geumpang basin northward to Krueng Raya on the Sumatra Island and Weh Island offshore (Fig. 1). We conducted a traditional geomorphic and geologic surveys along the fault. In 2015, we excavated a paleoseismic trench across the Seulimeum segment at Lamtamot. We also installed a geodetic alignment array to detect surface creep of the Seulimeum segment at Lamtamot. The method is the same as the one developed by San Francisco State University and USGS (Lienkaemper et al., 2014). We measured the array three times between 2013 and 2015.

3 Tectonic Setting and Previous Studies of the Northernmost Sumatran Fault

The Sumatran fault is a global example of arc-parallel strike-slip fault related to oblique plate subduction (Fitch, 1972; Yeats, 2012). The NW-trending Sumatran fault traverses the backbone range of the Sumatra Island for a length of 1900 km. Sieh and Natawidjaja (2000) published a detailed map of the Sumatran fault, and the map has been kept updated by incorporating new data and interpretations (Natawidjaja, 2018). However, there are relatively few geologic field studies of the Sumatran fault due mainly to limited accessibility to the areas. In our study area, Fernández-Blanco et al. (2016) conducted detailed structural and kinematic analyses of the faults on the islands offshore Banda Aceh. They proposed a strain partitioning along the two segments at the northern end of the Sumatran fault. Ghosal et al. (2012) mapped

the offshore extensions of the Aceh and Seulimeum segments based on seismic reflection profiles. Nonetheless, there were no studies that examined the tectonic landforms to reveal late Quaternary activity, geologic slip rate, and paleoseismicity, which are essential for seismic hazard analyses.

There was no paleoseismic trenching on the Aceh and Seulimeum segments. Besides, the recurrence interval of large earthquakes on individual segments of the Sumatran fault is poorly constrained (e.g., Bellier et al., 1997).

The historical seismic activity in the study area is relatively low (Fig. 1). Hurukawa et al. (2014) relocated historical moderate to large earthquakes since 1892 along the Sumatran fault and proposed that the Aceh and Seulimeum segments form a seismic gap. The 1935 M_s 7.0 earthquake was interpreted to have ruptured the northern Tripa segment south of the Aceh segment (Hurukawa et al., 2014). The 1964 M_b 6.7 earthquake may be associated with the Seulimeum segment (Sieh and Natawidjaja, 2000). The January 2013 M_w 6.1 earthquake was a right-lateral strike-slip event near the Geumpang and Tangse intramountain basins (Ito et al., 2016). The 2016 M_w6.6 Pidie Jaya earthquake caused considerable damage to the epicentral area with ~100 casualties. Salman et al. (2020) proposed that a previously unmapped northeast-trending left-lateral strike-slip fault is responsible for this event.

According to Bennett et al. (1981), the Barisan Mountains are underlain by rocks of Jurassic to Cretaceous age. Rocks of the same age underlie the mountains between the Aceh and Seulimeum segment. Post-Miocene sedimentary rocks underlie the rest of the area except around the Seulawah Agam volcano and the Weh Island, where Quaternary volcanic rocks overlie the basement rocks.

4 Geomorphic and Geologic Characteristics of the Aceh and Seulimeum Segments

The study area includes the Aceh and Seulimeum segments of the Sumatran fault. The 200-km-long Aceh segment lies on the northwestern extension of the Tripa segment and is separated from the Tripa segment by a 3-km-wide contractional step-over south of Takengon (Sieh and Natawidjaja, 2000). The Aceh segment extends N50°W and bounds the northeastern foot of the Barisan Mountains (Fig. 1).

The Seulimeum segment lies east of and branches northward from the Aceh segment. The southeastern end of the Seulimeum segment is located at ~4 km to the northeast of the Aceh segment at the northeastern edge of the Geumpang basin (Fig. 1). From there, the Seulimeum segment extends northwest (N40°W) for a distance of ~120 km. The fault traverses mountainous terrain between Geumpang and Lamtamot and cuts the southwestern slope of the Seulawah Agam volcano before reaching Krueng Raya. The Seulimeum segment extends offshore and cuts across the Weh Island (Sieh and Natawidjaja 2000). The Batee fault branches south-southeastward from the Aceh segment and is interpreted as a splay fault of the Sumatran fault (Sieh and Natawidjaja, 2000). The Batee fault is located at the topographic boundary between the Barisan Mountains and coastal lowlands (Fig. 1). Since we have not conducted extensive surveys for the Batee fault, we will not describe the fault in this paper.

In the following, we describe localities where clear geomorphic and geologic evidence of recent faulting is observed for the Aceh and Seulimeum segments from south to north

4.1 Aceh Segment

We conducted extensive fieldwork from the Geumpang basin northward. The Aceh segment bounds the southwestern margins of the elongated Geumpang and Tangse intramountain basins and Aceh basin. More than half of its length of this segment traverses mountainous terrain. Its trace is characterized by narrow valleys, systematic right-lateral deflections of stream channels, aligned saddles on mountain slopes, beheaded streams, and shutter ridges. The amount of right-lateral offset of streams is as large as 1 km.

The Aceh segment extends northwest into the Geumpang basin with a series of hill-side ridges and offset streams (Fig. 3a). At site 1 south of Geumpang downtown, the fault trace is marked by an uphill-facing (southwest-facing) scarp less than 20 m high cutting across a gently northeast-sloping surface (Photo 4a). Highly-weathered reddish rounded gravels as large as 50 cm in diameter are exposed on the surface. Between Geumpang and Mane, there are no apparent tectonic geomorphic features, and the exact location of the fault is unknown. At site 2 northwest of Mane, there is a ~1 km long, ~200 m wide, and ~20 m high linear ridge trending northwest and sticking out of the surrounding fluvial terraces. We interpret the fault bounds the sharp southwestern margin of the hill. During the M_w 6.1 earthquake on 21 January 2013, surface cracks appeared at two localities on and near the ridge, but we concluded that they resulted from slope failure. In the mountainous area between the Geumpang and Tangse basins, the fault is delineated by a series of shutter ridges and offset channels.

The Aceh segment bounds the southwestern margin of the Tangse basin filled with sediments shed by rivers flowing south to the Indian Ocean (Figs. 3b, 4b). At site 3, well-stratified river sediments dip ~35°E toward the fault. At site 4, an uphill-facing (southwest-facing) scarp ~5m high extends for ~300 m. At site 5 near Tangse downtown, there is an isolated hill with a veneer of highly weathered gravels. We interpreted that the fault extends along the northwest-trending linear trough that separates the hill from the mountain slope. In the northwest Tangse basin, the tectonic landform is obscured partly because of the vast amount of talus deposits and landslide debris. The Aceh segment extends further northwest to the southwestern margin of the Aceh basin. The linear valleys with stream offsets delineate the fault trace in the ~40-km-long stretch between the Tangse and Aceh basins, where the fault traverses the mountainous terrain.

The southwestern margin of the Aceh basin is not as sharp as those of the basins to the southeast. The fault is delineated by continuous uphill-facing (southwest-facing) scarps that cut the Plio-Pleistocene Seulimeum Formation of Bennett et al. (1981) that fills the basin (Fig. 3c). The scarps and linear troughs are continuous for ~20 km. The fault trace steps to the right about 500 m near the Keuliling Reservoir at Kuta Cot Glie. At site 6 (Krueng Jreue), the southwest-facing scarp trends N40°W and is ~10 m high (Fig. 4c). Siltstone exposed at the base of the scarp is extensively deformed with N30°W strike and 63°-78°NE dip. At site 7 (Aneuk Gle), a west-facing scarp and narrow valley on the downthrown side mark the fault (Fig. 4d). Modern rivers flow northeast, perpendicular to the scarps, suggesting that the scraps are tectonic in origin. Distinct fault scarp continues northwest for another 3 km from site 7.

We agree with Sieh and Natawidjaja (2000) that the Aceh segment lacks geomorphic evidence of late Quaternary activity along the northwestern margin of the Aceh basin (Figs. 1, 3c). We speculate that the Aceh segment becomes less active to the northwest, and the Seulimeum segment to the east accommodates most of the right-lateral shear of the Sumatran

fault. We checked two large outcrops near Banda Aceh (Fig. 1). Faults with a 3-m-wide well-developed brecciated zone within sandstone have attitudes of N60°W/81°NE and N59°W/75°NE at site 8 (Biluy). At site 9 (Gle Gurah), faults in limestone strike N85°W-N53°W. These faults in the bedrock trend more westerly than the Aceh segment and are not part of the Aceh segment's main fault zone. Offshore geophysical explorations by Ghosal et al. (2012) suggest that the Aceh segment lies several km east of the eastern shorelines of the Breueh and Nasi Islands. Therefore, we cannot preclude the possibility that the active Aceh segment extends further north but hidden beneath the recent deposits of the northern Aceh basin.

4.2 Seulimeum Segment

The Seulimeum segment extends northwestward from the northeastern margin of the Geumpang basin (Fig. 3a). The Seulimeum segment steps to the right for ~ 4 km from the Aceh segment. The Geumpang basin may be interpreted as a pull-apart basin. The fault bounds the southern margin of the Blang Pandak basin, a small intramountain basin (Fig. 3b). The fault trace around Blang Pandak follows the geologic boundary between metamorphic rocks to the north and intrusive rocks to the south (Bennett et al., 1981). Immediately west of the Seulimeum segment north of the Tangse basin, there is a drainage divide in valley between the river flowing south to the Indian Ocean and the river flowing north to the Malacca Strait (Fig. 3b). The north-flowing river has captured upstream leaches of the south-flowing river and is actively eroding its headwater. This stream piracy is possibly related to the movement of the Seulimeum segment.

At Kuala Panteue, between the divide and Krueng Seukeuek, a series of west-flowing stream channels are systematically offset right-laterally by the Seulimeum segment (Fig. 2a). The offset amounts are 60-180 m. Highly sheared (only ~30 % of basement rock structure is preserved), metasedimentary rocks are exposed on the channel floor along the fault (site 10, Fig. 4e). Shear planes in the basement trend N40°W to N60°W, parallel to the Seulimeum segment. Numerous landslides are observed within 100 m from the fault. Northwest of Krueng Seukeuek, the fault forms ~10-m-high uphill-facing (southwest-facing) fault scarp on alluvial fan surfaces (Fig. 3b). From here to Lamtamot, the fault trace is marked by aligned saddles and stream offsets in mountainous terrains where we have not carried out field surveys due to difficult accessibility.

We identified the most notable tectonic geomorphic features and fault outcrops at Lamtamot near the main road connecting Banda Aceh and Sigli (Fig. 3d). Here we conducted extensive fieldwork, including paleoseismic trenching. A ~1-km-long and southwest-facing fault scarp with a maximum height of 8 m cuts fluvial terraces formed by a southwest-flowing river (Figs. 2b, 4f). The scarp extends N30°W, almost perpendicular to the river's flowing direction, suggesting that the scarp is tectonic in origin. The scarp decreases its height to the northwest. We excavated a trench at the northern end of the scarp (Fig. 2b), as described below.

South of the river, there is a northwest-trending and ~20-m-high elongated ridge called the Kareung Hill (Fig. 2b). The fault passes at the southwestern margin of the hill, and the hill is interpreted as a pressure ridge. The hill is underlain by intercalated sandstone and mudstone correlated to the Padang Tiji Member of the Kota Bakti Formation of Bennett et al. (1981). There was a 45-m-long road cut across the hill that enabled us to examine the deformational features of the pressure ridge (site 11, Fig. 4g). We cleaned and gridded the outcrop every 1 m and logged it at a scale of 1:20 (Fig. 5). The strata are folded into a broad anticline and dip steeper closer to the Seulimeum segment. We mapped numerous normal faults, and they are classified into two. The faults west of the hinge trend WNW with north dip and are slightly oblique to the N30°W-

striking main fault. The faults east of the hinge trend almost N-S and dip steeply. These normal faults exhibit down-to-the-northeast displacement with less than 1 m stratigraphic offsets. They are probably associated with the anticlinal growth and movement of the Seulimeum segment. The faults that bound a graben at grid nos. 13-26 offset modern organic soil (Figs. 4h, 5), suggesting that they have moved in recent geologic time.

The Seulimeum segment is fully exposed to riverbank ~2 km south of the pressure ridge (site 12, Fig. 6). The sedimentary bedrock and semi-consolidated fluvial deposits are extensively deformed by several faults that form a 10-m-wide fault zone. The faults dip steeply and branch upward, typical characteristics for strike-slip faults. The easternmost fault dips steeply to the west and truncates extensively sheared sub-rounded to rounded gravels (Fig. 6c). There are several steeply east-dipping faults at the west end of the fault zone (Fig. 6b). A well-developed fault gauge ~30 cm thick is observed between these faults. Sandstone between the faults is extensively sheared, and portions close to the faults were transformed into fault gauge. This outcrop documents that the Sumatran fault is characterized by a broad and extensive shear zone reflecting its high activity and a large amount of total displacement.

Northwest of Lamtamot, the fault traverses the southwestern slope of the Seulawah Agam volcano (Fig. 3d). The fault forms upslope-facing (northeast-facing) fault scarps and linear depressions on the mountain slope covered mainly by blocks of hornblende andesite originated from lava or debris flows. At site 13, the fault scarp on an older surface is as high as 20 m. The scarp is 4m high on a younger surface at site 14, indicating repeated movement of the fault over time. Northwest of site 14, the Seulimeum segment traverses low relief volcanic terrain. The fault trace is delineated by linear toughs and closed depressions.

The fault extends to an elongated basin where the town of Krueng Raya is located (Fig. 3e). Near the southern end of the basin, the fault branches into a few strands and bounds the basin's eastern and western margins. The faults exhibit a left-stepping en echelon pattern. The eastern fault makes a linear depression and upslope-facing scarp at site 15. The fault on the west is marked by aligned saddles and a series of offset streams. The fault network is widely exposed to quarries of a pozzolan mine (site16). Several faults cut nonwelded and un-weathered pumice flow deposits. The main fault is accompanied by a well-developed 70-cm-thick fault gauge (Fig. 4i). The strike and dip of the fault are N18°W and 85°W. The dark brown gauge is clay-sized except near the host rock where breccia as large as 2 cm in diameter are scattered. This main fault is traceable northward on the quarry floor for ~ 50 m.

The Seulimeum segment extends offshore and onto the Weh Island, located at ~16 km northwest of the Sumatra Island (Fig. 1). Ghosal et al. (2012) analyzed the location and submarine structure of the Seulimeum segment based on seismic reflection profiling. The Weh Island is ~20 km long on the northwest-southeast direction and ~12 km wide on the northeast-southwest direction. The surface geology of the island is mostly composed of andesite of Quaternary age (Bennett at al., 1981) except for the northeastern part of the island, where several flights of flat surfaces are uplifted coral terraces (Fig. 3f). The Seulimeum segment cuts across the eastern part of the island from Balohan to Sabang. The fault trace is marked by southwest-facing fault scarp, linear depression, and right-lateral offset of streams. The N25°W-trending fault truncates uplifted coral terraces and remnants of volcanic cones located east of the fault.

The Seulimeum segment bounds the eastern margin of the Balohan Bay. At site 17, pumice flow deposits are cut by numerous faults. The fault that offsets all the strata (N10°W,

47°W) has a soft, 1-cm-thick fault gauge. The stream channel immediately south of the outcrop is offset right laterally at ~20 m. At site 18, well-stratified white pumice layers are cut by a fault (N56°W, 60°SW) with a ~2 mm thick fault gauge (Fig. 7). The amount of vertical offset is ~6 m down to the southwest, consistent with the uplifted marine terraces northeast of the fault. At site 19, immediately east of the main road connecting Balohan and Sabang, numerous faults offset well-consolidated andesite breccia. Near the western edge of the outcrop, a fault with an attitude of N26°W and 74°W is accompanied by ~40-cm-thick, blackish gray gauge easily broken by hand. In contrast, all the other faults exposed on the outcrop are accompanied by a consolidated gauge. At site 20, the fault is marked by a linear depression trending N20°W. The hill west of Sabang is composed of nonwelded, white to yellowish-white pumice, less than 10 cm in diameter. The fault sharply truncates the northeastern margin of the hill. Several steps of the flat-lying marine terraces east of the fault suggest that the fault's northeast side has uplifted. At site 21, the terrace surface is underlain by ~3-m-thick coral fragments, which overly unconformably andesite breccia less than 1 m in diameter.

In addition to the main Sumatran fault described above, Fernández-Blanco et al. (2016) mapped several subparallel faults and interpreted them as shear structures related to the main right-lateral faults. However, we could not identify geomorphic evidence of late Quaternary faulting along these subparallel faults.

5 Paleoseismic Trenching of the Seulimeum Segment at Lamtamot

5.1 Geomorphic Setting and Stratigraphy

Fluvial terraces along a southwest-flowing river are offset down-to-the-southwest at Lamtamot (Fig. 2b). The northwest-trending fault scarp attains its maximum height of ~8 m immediately northwest of the river. The scarp extends for ~600 m to the northwest, decreasing its height. We selected our trench site at a rice paddy field immediately northwest of the termination of the scarp (Figs. 2b, 8). We manually excavated a ~4 m long, ~1 m wide, and ~2 m deep trench in June 2015. We were not able to excavate deeper because of the high water table. The trench walls were almost vertical. We made 50-cm-interval grids on the north and south walls to facilitate logging at a scale of 1:10. We also made photo mosaics of the walls. To date the timing of paleoseismic events, we sampled charcoals and woods for radiocarbon dating (Table 1).

Fluvial sediments exposed on the trench walls were displaced by several fault branches (Fig. 9). The faults show the vertical component of motion down to the southwest consistent with the southwest-facing fault scarp. At the bottom of the trench, pale-yellow, medium-grained sandstone bedrock was exposed on the up-thrown side of the fault. Clasts in the sediments were mostly sandstone with occasional andesitic rocks. We divided the strata from unit 0 to unit 100. Table 2 lists brief descriptions of the strata and their ages.

5.2 Fault Structure and Paleoseismic Events

Several faults were exposed between N2 and N3 on the north wall and between S1 and S2 on the south wall. At the bottom of the walls, the fault zone is 30 cm wide, while it is ~60 cm wide on the upper portion of the wall. At the trench bottom, there are 2-3 faults, and they branch upward. The fault zone's overall dip is 80°W, while some of the branch faults dip near vertical or steeply to the east. The geometry of the faults is consistent with the geomorphic observations that

the Sumatran fault is predominantly a strike-slip fault. The sense of vertical component of movement is down to the west. The older strata are offset more than the younger strata suggesting repeated movement of the faults.

The youngest strata cut by the faults is unit 20. The faults terminate up section at different stratigraphic horizons, and vertical stratigraphic separation of the units is more significant for older strata. From these structural observations, we identified geologic evidence for four paleoseismic events on the trench walls.

Event 1: The most recent faulting event occurred sometime during the deposition of unit 20. The faults offset the boundary between unit 20 and unit 30. The lower portion of unit 20 is offset, as evidenced by the truncation of channel deposits on the north wall. The faults do not offset the boundary between unit 10 and unit 20, suggesting that the event occurred during the deposition of unit 20. The vertical displacement associated with this event is ~20 cm based on the stratigraphic offset of the upper boundary of unit 30 on both walls.

Event 2: The penultimate event occurred sometime during the deposition of unit 40. On the south wall, a few faults offset the boundary between unit 40 and unit 50, but they disappear within unit 40. On the north wall, there is a fault that is overlain by unit 30. The vertical offset of the upper boundary of unit 50 is 40-50 cm, suggesting that the vertical displacement associated with event 2 was 20-30 cm.

Event 3: The anti-penultimate event occurred sometime during the deposition of unit 50. On both walls, some faults cut the base of unit 50 but terminate within the unit. The stratigraphic offset of the top of unit 60 is 70-100 cm across the fault zone, which is more significant than that of the upper horizons, although the top of unit 60 is not an ideal reference due to channel erosion by the overlying unit 50.

Event 4: Event 4 occurred sometime during the deposition of unit 60. On both walls, some faults juxtapose unit 60 and unit 70 but disappear within unit 60. We cannot estimate the vertical offset of the lower boundary of unit 60 because it is only partially exposed on the fault zone's upthrown side.

There is no evidence of older events because no fault terminates within the older stratigraphic horizons.

6 Geodetic Creep Monitoring of the Seulimeum Segment at Lamtamot

Ito et al. (2012) identified aseismic creep of the Sumatran fault at a rate of 20 ± 6 mm/yr near the southern end of our study area. To detect aseismic surface creep, we conducted an alignment array survey across the Seulimeum segment at Lamtamot. We adopted the same method used to monitor surface creep for the right-lateral strike-slip faults in the San Francisco Bay area (Lienkaemper et al., 2014). We installed three benchmarks ~100 m apart from one another; two on one side of the fault and one on the other side of the fault. We then repeatedly measured the angle made by the three benchmarks using a total station, Leica TPS 1201, that has an angle measurement accuracy of 1”. We installed the benchmarks and conducted the first measurement on 12 November 2013. We repeated the measurement on 26 September 2014 and 6 June 2015. During the 570 days between the first and third measurements, we detected a 3.0 ± 0.8 mm fault-parallel, right-lateral movement across the fault. The value is above the minimum detection level of our measurement and translates to a 1.9 ± 0.5 mm/yr right-lateral surface creep rate of the Seulimeum segment at Lamtamot.

7 Discussion

7.1 Timing and Recurrence Interval of Surface-Rupturing Earthquakes on the Seulimeum Segment

We modeled the paleoseismic history of the Seulimeum segment using the stratigraphic information and ages of strata based on OxCal 4.3 (Bronk Ramsey, 2009) (Fig. 10). Because we were able to date only units 20, 50, 80, and 90, we could not date the individual events except for the oldest event (event 4). The latest event predates the earliest earthquake cataloged for the area, 1892 (Hurukawa et al., 2014). We are sure that events 1 and 2 occurred after the deposition of unit 50. Because event 3 occurred sometime during the deposition of unit 50, it is impossible to determine whether samples 1 and 18 predate or postdate event 3. For this modeling, we assumed that event 3 postdates the two samples. The timing of event 4 is constrained between AD1265 and 1365. This modeling suggests that four surface-rupturing events occurred after AD1265-1365 and before AD1892. The average recurrence interval of the surface-rupturing earthquake on the Seulimeum segment is calculated at 130-210 years.

The only historical $M \geq 6$ earthquake near the Seulimeum segment is the 1964 M_b 6.7 earthquake, whose epicenter is placed slightly offshore Banda Aceh (Fig. 1; Hurukawa et al., 2014). Sieh and Natawidjaja (2000) suggested that the Seulimeum segment may have generated this event because Krueng Raya was damaged more severely than Banda Aceh. During the fieldwork, we interviewed a Lamtamot resident who was the 2nd year elementary school student at the time of the 1964 earthquake. He described more than 100 houses at Lamtamot were collapsed or damaged, but none was killed. Because the faults on the trench walls terminate within unit 20 and the overlying strata are not faulted, we conclude that the Seulimeum segment near Lamtamot has not ruptured the surface during the 1964 earthquake.

7.2 Late Quaternary Faulting and Seismic Hazard of the Sumatran Fault

We identified distinct tectonic landforms along the entire length of the Sumatran fault north of the Geumpang basin. As documented by previous studies (e.g., Sieh and Natawidjaja, 2000; Ito et al., 2012; Fernández-Blanco et al., 2016), the slip on the Sumatran fault is predominantly right-lateral strike-slip, which is clearly shown by systematic right-lateral deflections of stream channels. The direction of vertical movement changes from place to place, and the faults exposed on the outcrops and trench walls dip steeply to vertical. These are common characteristics of strike-slip faults.

In this study, we could not obtain a geologic slip rate. Aseismic creep rates of ~20 mm/yr for the Aceh segment were estimated by Ito et al. (2012) and Tong et al. (2018) based on geophysical methods. We agree with such a high slip rate based on clear and fresh tectonic landforms and a short recurrence interval of seismic events. However, we found no evidence that creeping of this magnitude is occurring at the surface. We paid close attention to the deformation of artificial features on the fault trace during the fieldwork but found none. The alignment array survey at Lamtamot indicated only ~2 mm/yr right-lateral creep. The trenching at Lamtamot clearly shows that the fault ruptured the surface intermittently, not by continuous creep. These observations suggest that the faults in the study area rupture the surface during moderate to large earthquakes.

The discrepancy between the geophysical observations and our field observations is possibly related to the difference in spatial scales and resolutions. Our creep monitoring array

spans ~100 m across the fault trace, whereas the GNSS sites near the fault are apart from one another more than several km. Ito et al. (2019) expanded their GNSS network to monitor slip on the Seulimeum segment near Banda Aceh in August 2017. They repeated the measurements in January 2019 and August 2019. Based on the data, they detected a 15mm/yr rigid block motion across the Seulimeum segment. The coupling ratio and slip deficit rate around Lamtamot is estimated at ~0.6 and ~9 mm/yr, respectively. This significant slip deficit rate agrees with our geologic field observations that the Seulimeum segment ruptures the surface during moderate to large earthquakes.

Based on relocations of large historical earthquakes along the Sumatran fault, Hurukawa et al. (2014) concluded that the Aceh and Seulimeum segments have not ruptured since 1892. In contrast, the Tripa segment immediately to the south of the Aceh segment ruptured during the 1935 (M_s 7.0) and 1936 (M_s 7.2) earthquakes. Hurukawa et al. (2014) pointed out that the Aceh and Seulimeum segments form seismic gaps and may produce M_s ~7.4 earthquakes. The elapsed time since the last faulting event on these faults is more than 120 years. Because the average recurrence interval of the surface-rupturing earthquakes on the Seulimeum segment was estimated at 130-210 years, the seismic potential of the northernmost Sumatran fault is high.

The Aceh Province is vulnerable to shallow inland earthquakes as evidence by recent moderate events that caused considerable loss of lives: ~50 casualties by the 2013 M_w 6.1 Tanah Gayo earthquake and ~100 causalities by the 2016 M_w 6.6 Pidie Jaya earthquake. A massive earthquake on the Sumatran fault, especially near the population centers like Banda Aceh, would likely cause much more extensive damage. Landslides appear to be one of the most devasting geologic hazards during large earthquakes on the fault, as repeatedly observed during massive earthquakes in mountainous regions such as the 2005 Kashmir earthquake (Kaneda et al., 2008). The Aceh segment runs along the base of the steep northeastern slope of the Barisan Mountains. There are numerous landslide scars on the slope and large debris and talus deposits at the foot of the mountains. Because the rivers flow the base of the mountains forming narrow gouges, landslide debris would quickly dam these rivers and flood the intramountain basins like the Geumpang and Tangse basins.

8 Conclusions

In this paper, we presented the results of our geologic investigations of the Aceh and Seulimeum segments of the Sumatran fault north of the latitude of N4°45’. These segments have not ruptured in the past 120 years and form seismic gaps. We mapped these faults based on interpretations of the ALOS/PRISM images and geologic fieldworks. We also used various maps based on the DEMNAS. Conspicuous tectonic landforms document that these segments are predominantly right-lateral strike-slip faults with repeated movement in the late Quaternary. The trenching survey of the Seulimeum segment at Lamtamot provided evidence of four surface-rupturing earthquakes that occurred after AD1265-1365 and before AD1892. The average recurrence interval of the surface-rupturing earthquake is calculated at 130-210 years. The elapsed time since the last faulting event on these faults is more than 120 years. We interpret that the probability of a massive earthquake on the northernmost Sumatran fault is high.

Acknowledgments

We thank Syiah Kuala University students for their assistance in the field and the landowner of the Lamtamot trench site to conduct trenching in his property. Nobuhisa Matsuta joined a field

campaign and took aerial photos using a drone. Jim Lienkaemper kindly instructed HT on the geodetic creep monitoring method. We are also grateful to Takeo Ito for the information on their GNSS measurements and Adi Patria for the critical review of an early version of the manuscript. This study was supported by the Grant-in-Aid for Scientific Research (B) No. 24403005 and 17H04577 to TT from Japan Society of the Promotion of Science. The data related to this research is available at https://osf.io/ytz84/.

References

Bellier, O., Sébrier, M, Pramumijoyo, S., Beaudouin, Th., Harjono, H., Bahar, I. and Forni, O. (1997). Paleoseismicity and seismic hazard along the Great Sumatran Fault (Indonesia), *Journal of Geodynamics, 24*, 169-183. https://doi.org/10.1016/S0264-3707(96)00051-8

Bennett, J. D., Bridge, D. McC., Cameron, N. R., Djunuddin, A., Ghazali, S. A., Jeffery, D. H., Kartawa, W., Keats, W., Rock, N. M. S., Thomson, S. J. and Whandoyo, R. (1981). *Geologic map of the Bandaaceh Quadrangle, Sumatra, scale 1:250,000*, Geological Research and Development Centre, Indonesia.

Bronk Ramsey, C. (2009). Bayesian analysis of radiocarbon dates, *Radiocarbon, 51*, 337-360. https://doi.org/10.1017/S0033822200033865

Dziewonski, A. M., Chou, T. A. and Woodhouse, J. H. (1981). Determination of earthquake source parameters from waveform data for studies of global and regional seismicity, *Journal of Geophysical Research, 86*, 2825-2852. https://doi.org/10.1029/JB086iB04p02825

Ekström, G., Nettles, M. and Dziewonski, A. M. (2012). The global CMT project 2004-2010: Centroid-moment tensors for 13,017 earthquakes, *Physics of the Earth and Planetary Interiors, 200-201*, 1-9. https://doi.org/10.1016/j.pepi.2012.04.002

Fernández-Blanco, D., Philippon, M. and von Hagke, C. (2016). Structure and kinematics of the Sumatran Fault System in North Sumatra (Indonesia), *Tectonophysics, 693*, 453-464. https://doi.org/10.1016/j.tecto.2016.04.050

Fitch, T. J. (1972). Plate convergence, transcurrent faults, and internal deformation adjacent to Southeast Asia and the western Pacific, *Journal of Geophysical Research, 77*, 4432–4460. https://doi.org/10.1029/JB077i023p04432

Ghosal, D., Singh, S. C., Chauhan, A. P. S. and Hananto, N. D. (2012). New insights on the offshore extension of the Great Sumatran fault, NW Sumatra, from marine geophysical studies, *Geochemistry Geophysics Geosystems, 13*, Q0AF06. https://doi.org/10.1029/2012GC004122

Hurukawa, N., Wulandari, B. R. and Kasahara, M. (2014). Earthquake history of the Sumatran fault, Indonesia, since 1892, derived from relocation of large earthquakes, *Bulletin of the Seismological Society of America, 104*, 1750-1762. https://doi.org/10.1785/0120130201

Ito, T., Gunawan, E., Kimata, F., Tabei, T., Simons, M., Meilano, I., Agustan, Ohta, Y., Nurdin, I. and Sugiyanto, D. (2012). Isolating along-strike variations in the depth extent of shallow creep and fault locking on the northern Great Sumatran Fault, *Journal of Geophysical Research, 117*, B06409. https://doi.org/10.1029/2011JB008940

Ito, T., Gunawan, E., Kimata, F., Tabei, T., Meilano, I, Agustan, Ohta, Y., Ismail, N., Nurdin, I. and Sugiyanto, D. (2016). Co-seismic offsets due to two earthquakes (Mw 6.1) along the

Sumatran fault system derived from GNSS measurements, *Earth, Planets and Space, 68:57*. https://doi.org/10.1186/s40623-016-0427-z

Ito, T., Kimura, H., Tabei, T., Okubo, M., Yamashina, T., Kimata, F., Pratama, C., Agustan, Umar, M., Ismail, N., Sugiyanto, D. and Nurdin, I. (2019). Block motion model based on GNSS observation around Banda Aceh, Indonesia, *Abstract of the 132nd Meeting of the Geodetic Society of Japan*, 207-208. (in Japanese)

JAXA (Japan Aerospace Exploration Agency) (2007). *NDX-070015 ALOS User handbook*. http://www.eorc.jaxa.jp/ALOS/en/doc/alos userhb en.pdf

Kaneda, H., Nakata, T., Tsutsumi, H., Kondo, H., Sugito, N., Awata, Y., Akhtar, S. S., Majid, A., Khattak, W., Awan, A. A., Yeats, R. S., Hussain, A., Ashraf, M., Wesnousky, S. G. and Kausar, A. B. (2008). Surface rupture of the 2005 Kashmir, Pakistan, earthquake and its active tectonic implications, *Bulletin of the Seismological Society of America, 98*, 521-557. https://doi.org/10.1785/0120070073

Lienkaemper, J. J., McFarland, F. S., Simpson, R. W. and Caskey, S. J. (2014). Using surface creep rate to infer fraction locked for sections of the San Andreas fault system in northern California from alignment array and GPS data, *Bulletin of the Seismological Society of America, 104*, 3094-3114. https://doi.org/10.1785/0120140117

McCloskey, J., Nalbant, S. S. and Steacy, S. (2005). Earthquake risk from co-seismic stress, *Nature, 434*, 291. https://doi.org/10.1038/434291a

Natawidjaja, D. H. and Triyoso, W. (2007). The Sumatran fault zone – from source to hazard, *Journal of Earthquake and Tsunami, 1*, 21-47. https://doi.org/10.1142/S1793431107000031

Natawidjaja, D. H. (2018). Updating active fault maps and sliprates along the Sumatran Fault Zone, Indonesia, *IOP Conference Series: Earth and Environmental Science*, *118*, 012001. doi: 10.1088/1755-1315/118/1/012001

Salman, R., Lindsey, E. O., Feng, L., Bradley, K., Wei, S., Wang, T., Daryono, M. R. and Hill, E. M. (2020). Structural controls on rupture extent of recent Sumatran Fault Zone earthquakes, Indonesia, *Journal of Geophysical Research, 125*, e2019JB018101. https://doi.org/10.1029/2019JB018101

Sieh, K. and Natawidjaja, D. (2000). Neotectonics of the Sumatran fault, Indonesia, *Journal of Geophysical Research, 105*, 28295-28326. https://doi.org/10.1029/2000JB900120

Tabei, T., Kimata, F., Ito, T., Gunawan, E., Tsutsumi, H., Ohta, Y., Yamashina, T., Soeda, Y., Ismail, N., Nurdin, I., Sugiyanto, D. and Meilano, I. (2015). Geodetic and geomorphic evaluations of earthquake potential of the northern Sumatran fault, Indonesia, *International Association of Geodesy Symposia*. https://doi.org/10.1007/1345_2015_200

Tong, X., Sandwell, D. T. and Schmidt, D. A. (2018). Surface creep rate and moment accumulation rate along the Aceh segment of the Sumatran fault from L-band ALOS-1/PALSAR-1 observations, *Geophysical Research Letters, 45*, 3404-3412. https://doi.org/10.1002/2017GL076723

Yeats, R. (2012). *Active Faults of the World*, Cambridge University Press, 621 p.

528 **Table 1.** Radiocarbon ages for samples from the Lamtamot trench. All samples were pretreated
529 by acid/alkali/acid washes.

530 **Table 2.** Description of stratigraphic units of the Lamtamot trench.

531 **Figure 1** Index map of the study area. Solid lines are simplified traces of the Sumatran and Batee
532 faults based on the interpretation of stereo-paired ALOS/PRISM images. The rectangles denote
533 the locations of Figs. 3a-f. The stars show the epicenters of historical crustal earthquakes ($M \geq$
534 6.0) since 1892 from Hurukawa et al. (2014). These are the 1935 (M_s 7.0), 1964 (M_b 6.7), and
535 1967 (M_b 6.1) earthquakes. The focal mechanism solutions are for the earthquakes greater than
536 M_w 6.0 and shallower than 30 km depth since 1976 from the global CMT catalog (Dziewonski et
537 al., 1981; Ekström et al., 2012). These are the 2013 earthquake near Geumpang (M_w 6.1) and
538 2016 Pidie Jaya earthquake (M_w 6.6). The background shaded relief map was constructed using
539 the DEMNAS data.

540 **Figure 2** Stereographic ALOS/PRISM images along the Seulimeum segment. (a) Systematic
541 right-lateral stream offsets (white dotted lines) at Kuala Panteue. The black dashed line indicates
542 the fault trace. (b) Tectonic geomorphic features at Lamtamot. The filled box denotes the trench
543 site. The location of each figure is shown in Figs. 3b and 3d. Modified from Tabei et al. (2015).

544 **Figure 3** Detailed active fault map of the northernmost Sumatran fault in Aceh. The location of
545 each figure is shown in Fig. 1. The base map is a shaded relief map constructed from the
546 DEMNAS. Thick black lines denote fault trace; dashed where the location is indistinct. u:
547 upthrown side. d: downthrown side. White lines denote offset streams.

548 **Figure 4** Field photographs of tectonic landforms and outcrops. Red arrows denote active faults.

549 **Figure 5** Log of the outcrop across the Kareung Hill at Lamtamot. We used the "Stereonet
550 version 9.9.6" developed by Richard W. Allmendinger to plot the bedding planes and faults on
551 the equal-area stereo net.

552 **Figure 6** Fault outcrop at riverbank ~2 km south of the Kareung Hill, Lamtamot (site 12).
553 Yellow lines and arrows indicate faults.

554 **Figure 7** Fault outcrop east of Balohan on the Weh Island (site 18).

555 **Figure 8** The Lamtamot trench site. (a) Photograph showing the location of the trench at the
556 northern end of the southwest-facing fault scarp. (b) Topographic map around the trench site
557 constructed by a total station survey. (c) Photograph of the ~4-m-long and ~2-m-deep hand-dug
558 trench.

559 **Figure 9** Log of the north and south walls of the Lamtamot trench. Numerals in red are ^{14}C ages
560 in yBP.

561 **Figure 10** An OxCal modeling of paleoseismic events on the Seulimeum segment at Lamtamot.

562
563

Figure 1.

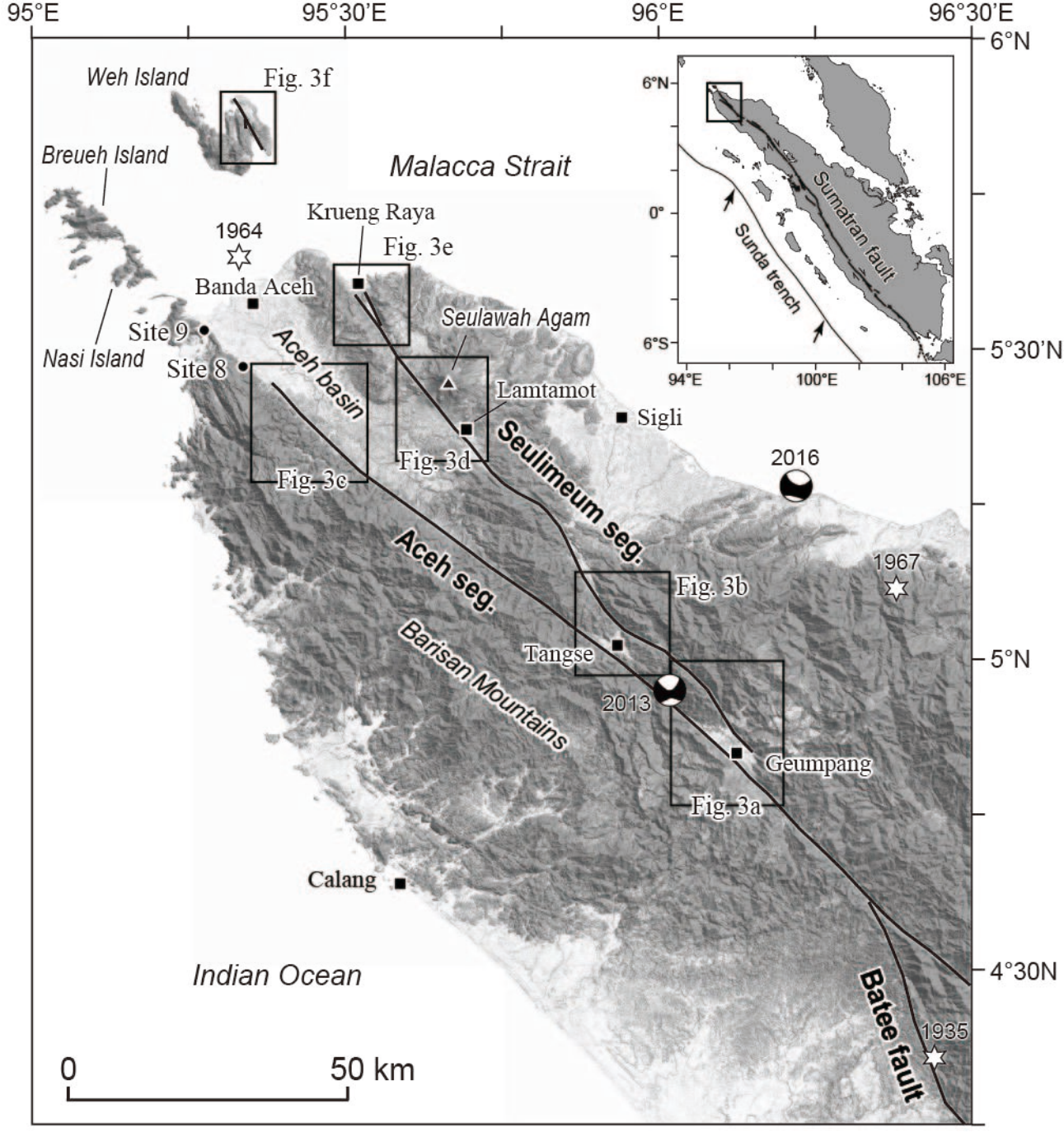
95°E
95°30'E
96°E
96°30'E
6°N
5°30'N
5°N
4°30N
Weh Island
Fig. 3f
Breueh Island
Malacca Strait
Krueng Raya
Fig. 3e
1964
Banda Aceh
Site 9
Site 8
Nasi Island
Seulawah Agam
Aceh basin
Lamtamot
Sigli
Fig. 3d
Fig. 3c
Seulimeum seg.
2016
Aceh seg.
1967
Fig. 3b
Barisan Mountains
Tangse
2013
Geumpang
Fig. 3a
Calang
Indian Ocean
Batee fault
1935
0
50 km
6°N
0°
6°S
94°E
100°E
106°E
Sumatran fault
Sunda trench

Fig. 1

Figure 2.

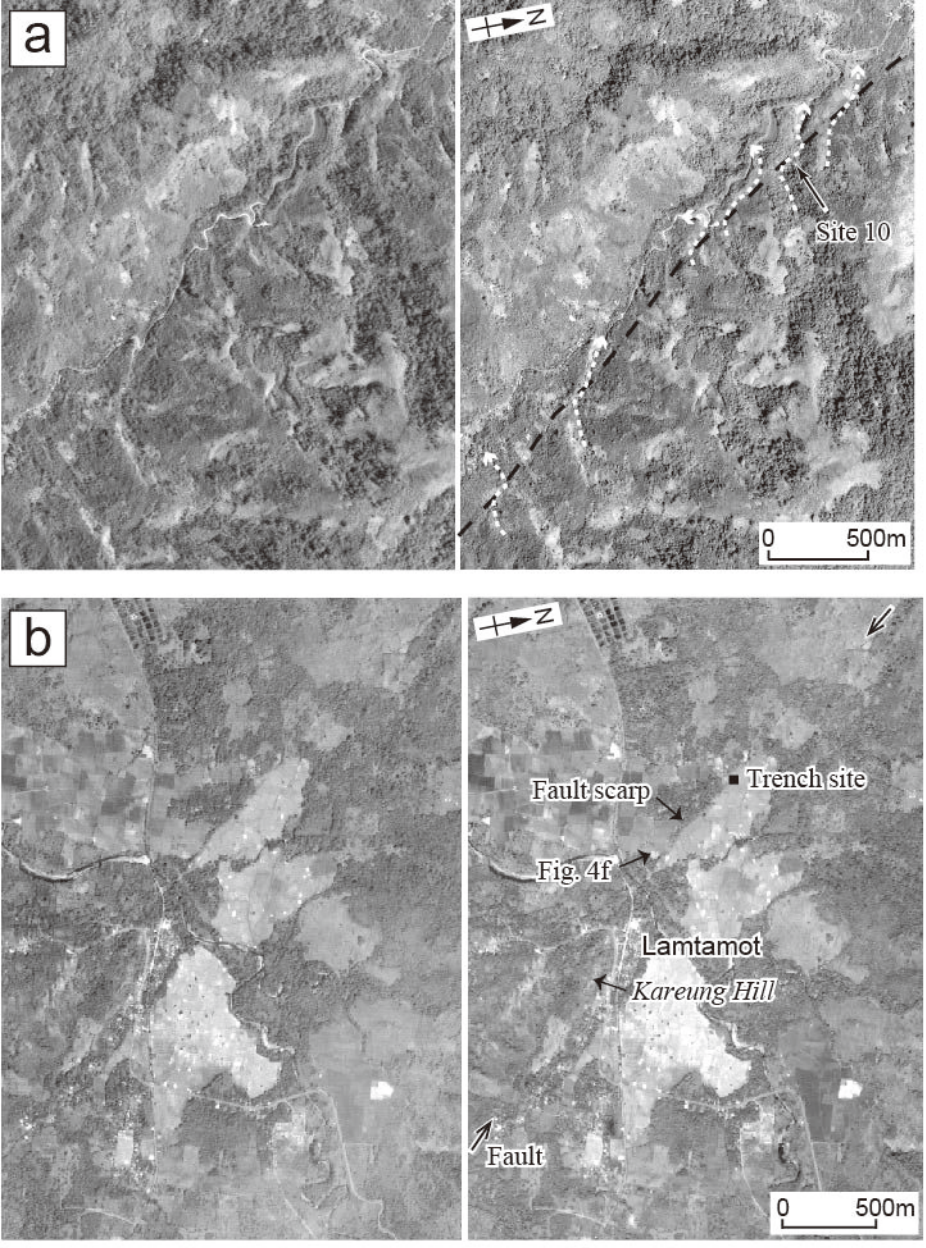
a
N
Site 10
0
500m
b
N
Fault scarp
Trench site
Fig. 4f
Lamtamot
Kareung Hill
Fault
0
500m

Fig. 2

Figure 3a.

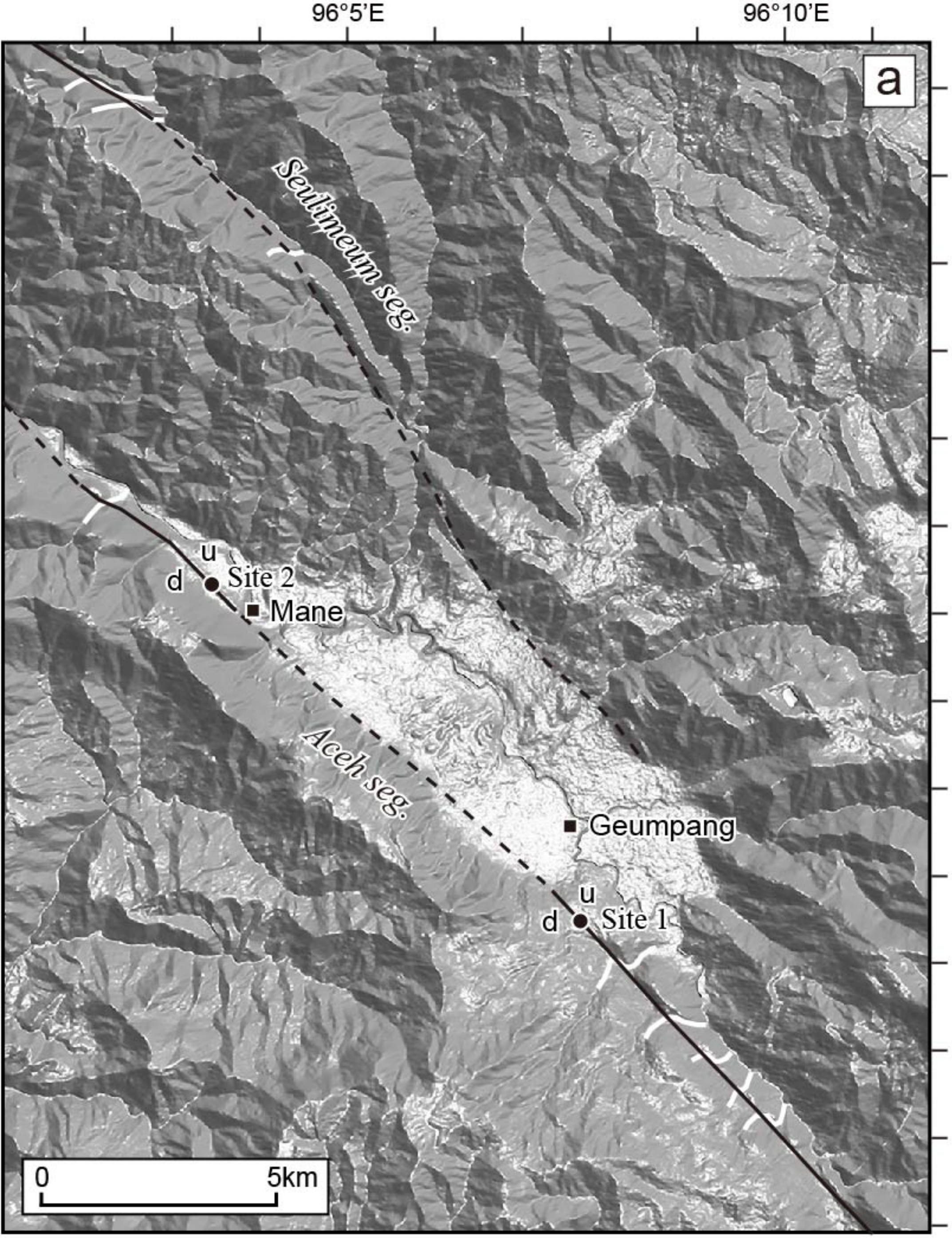
96°5'E
96°10'E
a
Seulimeum seg.
u
d
Site 2
Mane
Aceh seg.
Geumpang
u
d
Site 1
4°55'N
4°50'N
0
5km

Fig. 3a

Figure 3b.

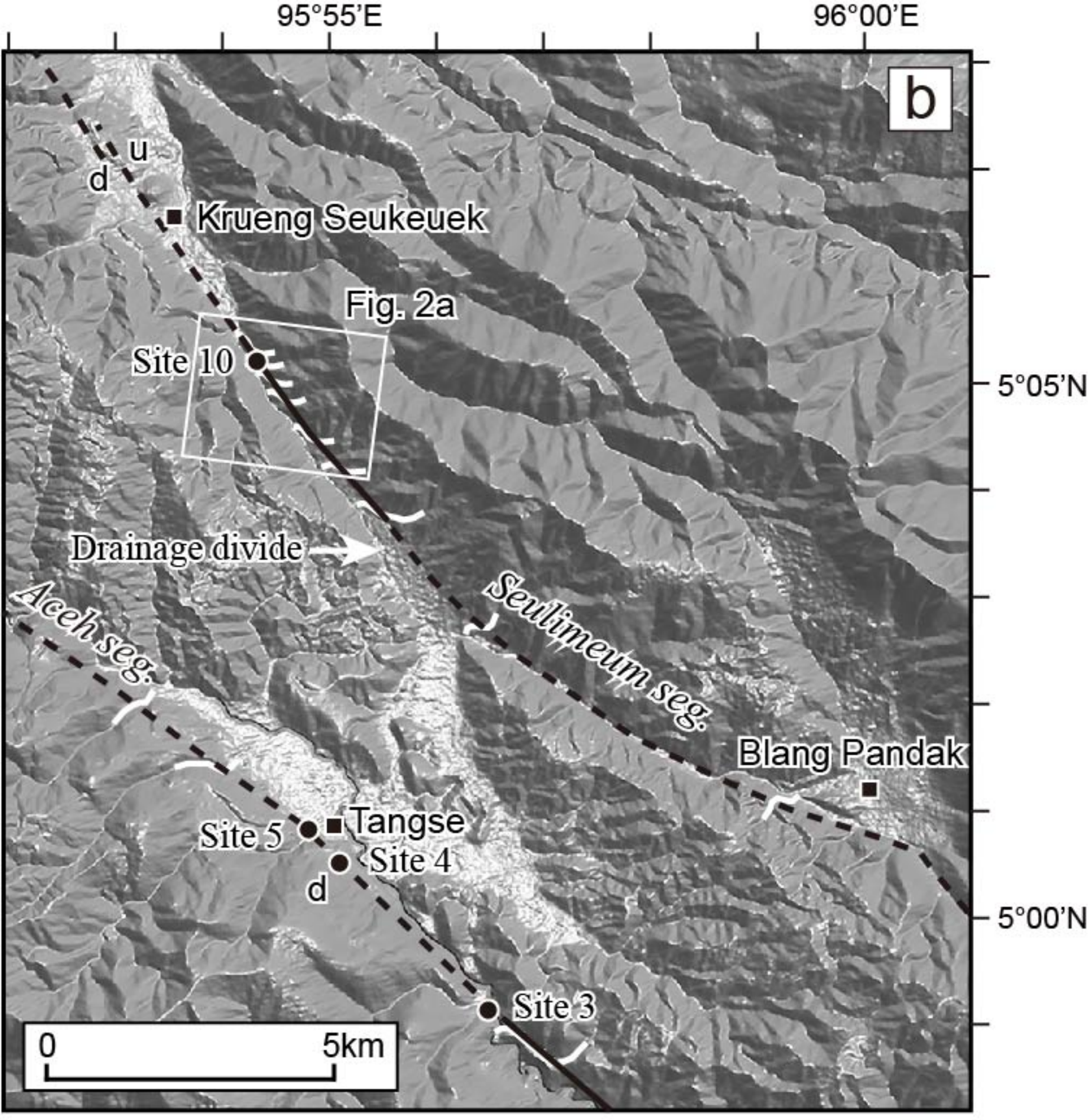
95°55'E
96°00'E
b
u
d
Krueng Seukeuek
Fig. 2a
Site 10
5°05'N
Drainage divide
Aceh seg.
Seulimeum seg.
Blang Pandak
Site 5
Tangse
Site 4
d
5°00'N
Site 3
0
5km

Fig. 3b

Figure 3c.

95°25'E

95°30'E

C

Aceh basin

u

d

u

d

Site 7

Site 6

d

u

Keuliling Res.

Aceh seg.

5°25'N

5°20'N

0

5km

Fig. 3c

Figure 3d.

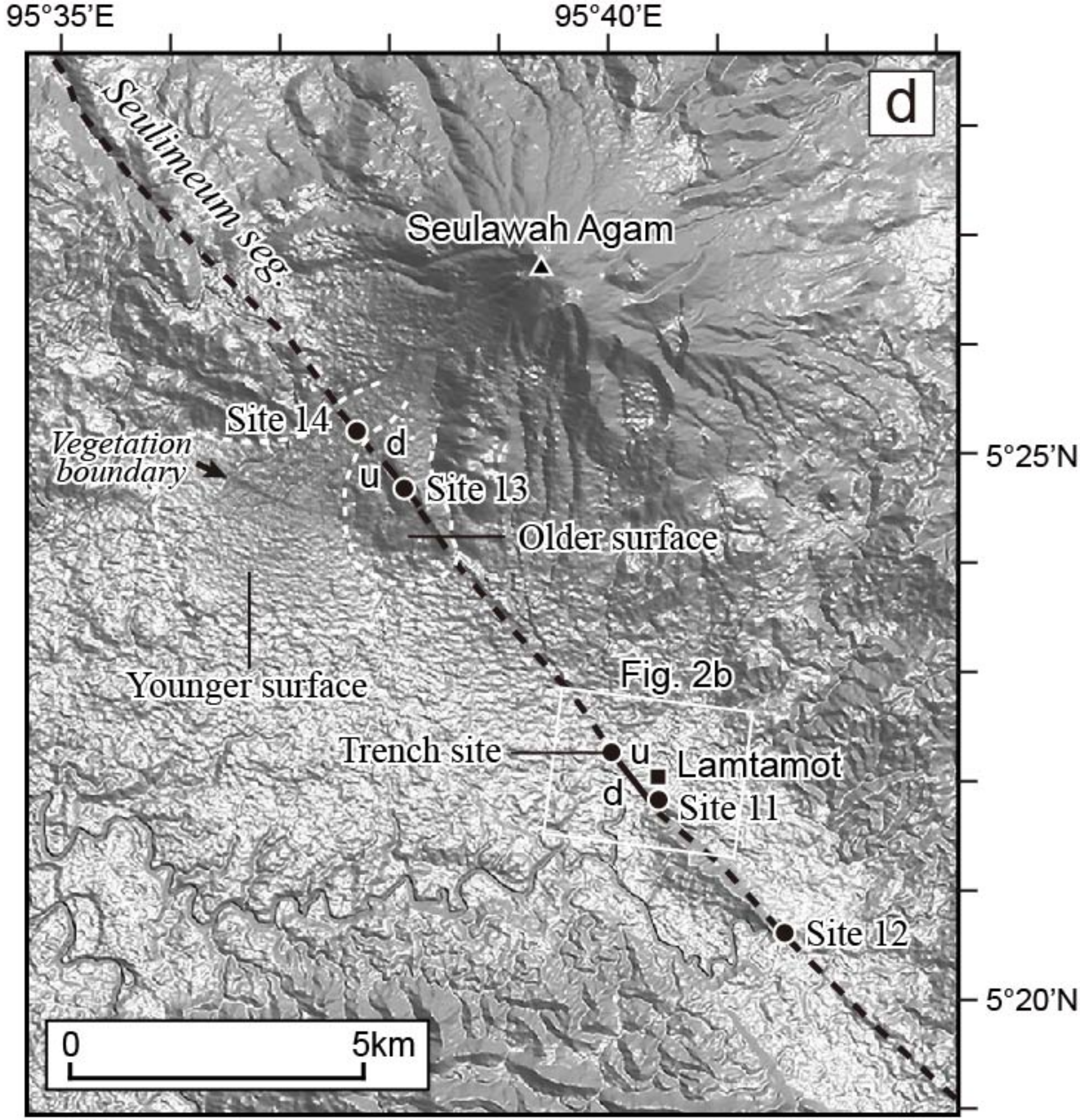
95°35'E
95°40'E
5°25'N
5°20'N
d
Seulimeum seg.
Seulawah Agam
Site 14
d
u
Site 13
Vegetation boundary
Older surface
Younger surface
Fig. 2b
Trench site
u
Lamtamot
d
Site 11
Site 12
0
5km

Fig. 3d

Figure 3e.

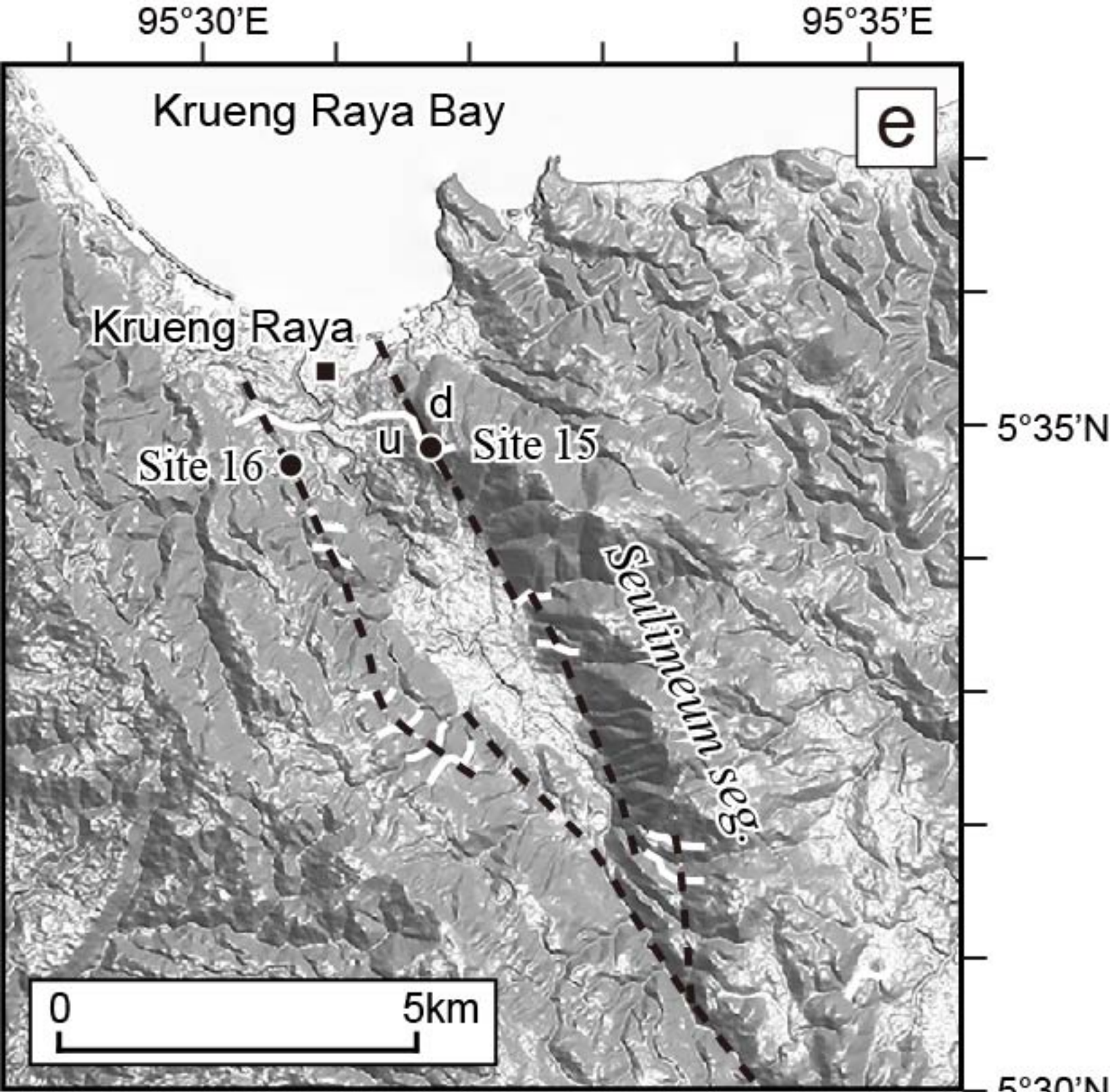
95°30'E
95°35'E
Krueng Raya Bay
e
Krueng Raya
d
u
Site 15
Site 16
Seulimeum seg.
0
5km
5°35'N
5°30'N

Fig. 3e

Figure 3f.

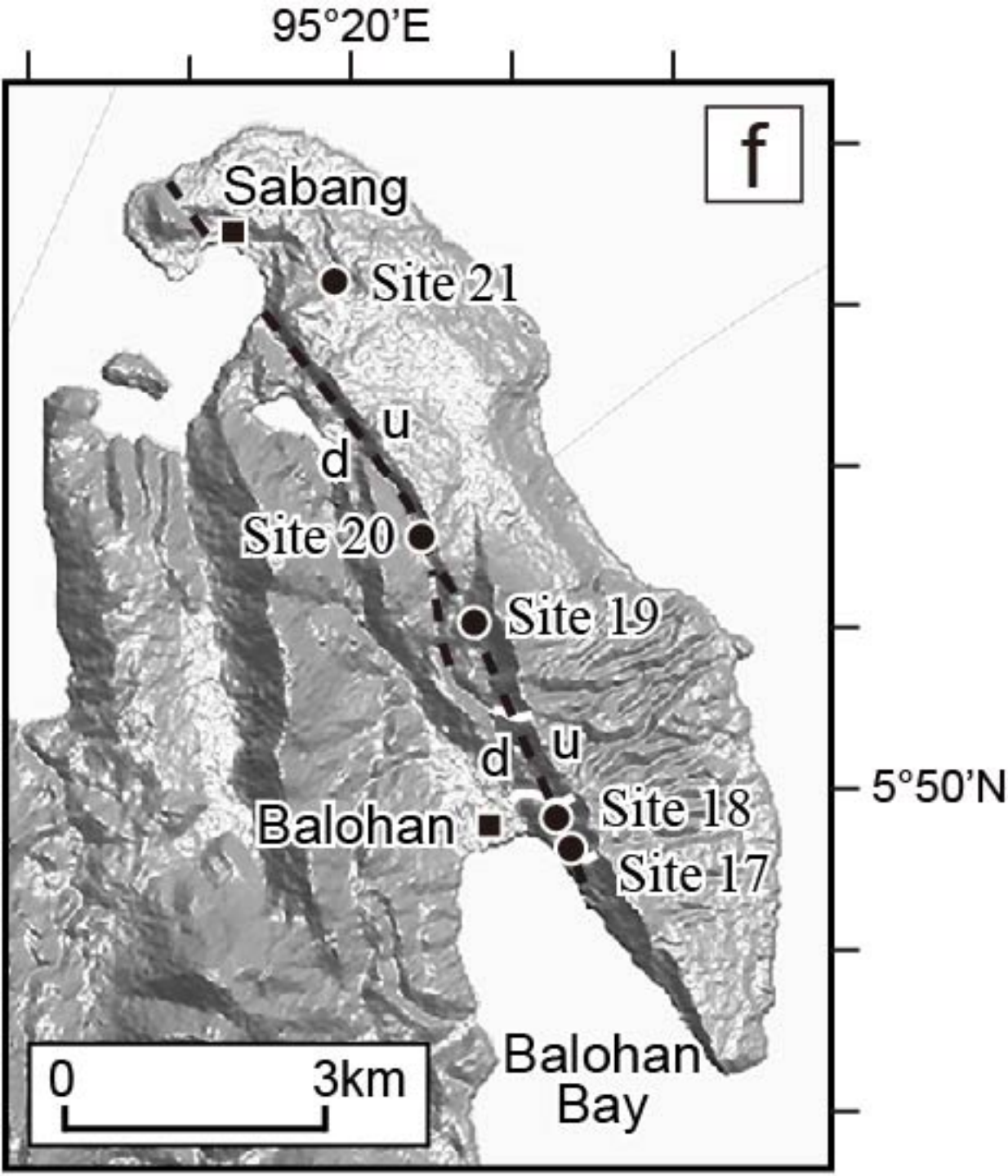
95°20'E
f
Sabang
Site 21
u
d
Site 20
Site 19
d
u
Balohan
Site 18
Site 17
5°50'N
0
3km
Balohan
Bay

Fig. 3f

Figure 4.

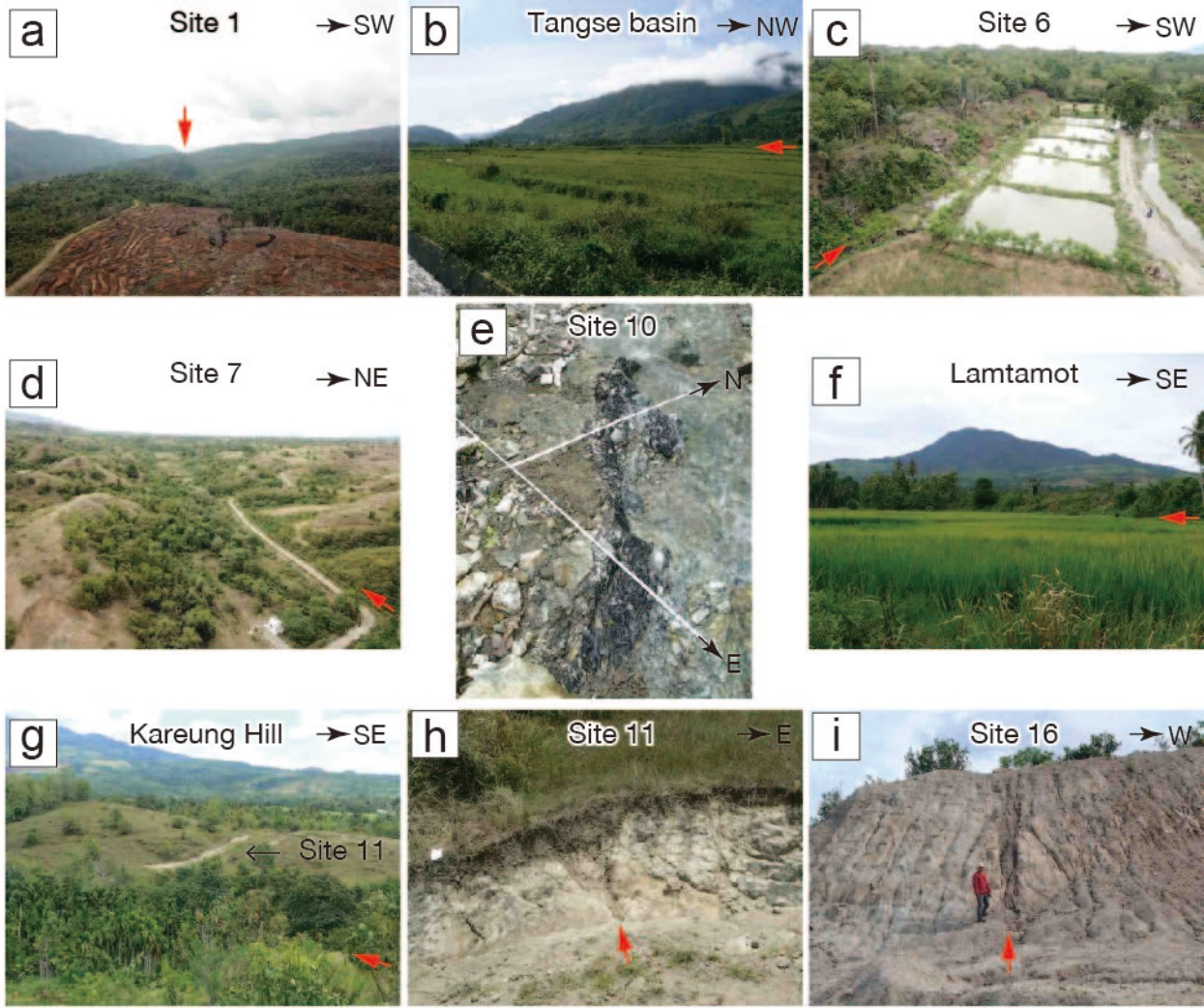
a
Site 1
SW
b
Tangse basin
NW
c
Site 6
SW
d
Site 7
NE
e
Site 10
N
E
f
Lamtamot
SE
g
Kareung Hill
SE
Site 11
h
Site 11
E
i
Site 16
W

Fig. 4

Figure 5.

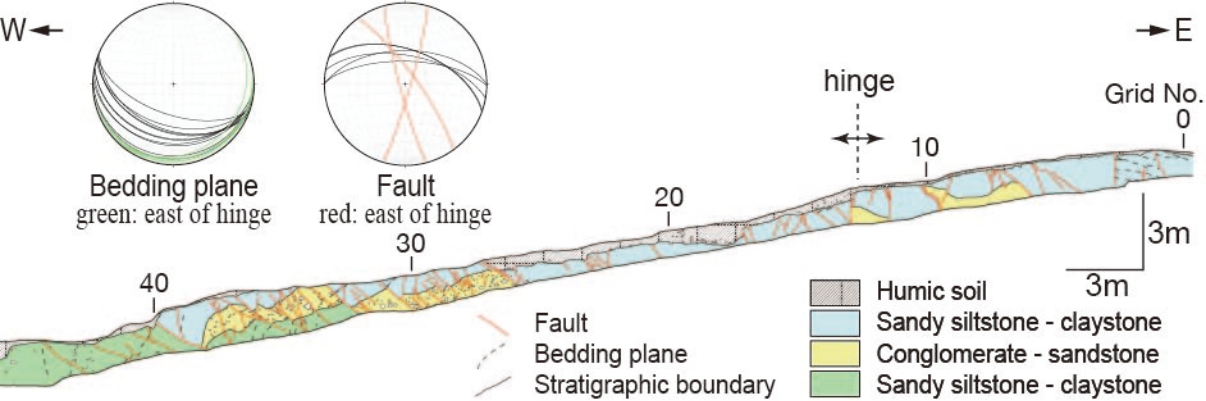
W
E
Bedding plane
green: east of hinge
Fault
red: east of hinge
hinge
Grid No.
0
10
20
30
40
3m
3m
Humic soil
Sandy siltstone - claystone
Conglomerate - sandstone
Sandy siltstone - claystone
Fault
Bedding plane
Stratigraphic boundary

Fig. 5

Figure 6.

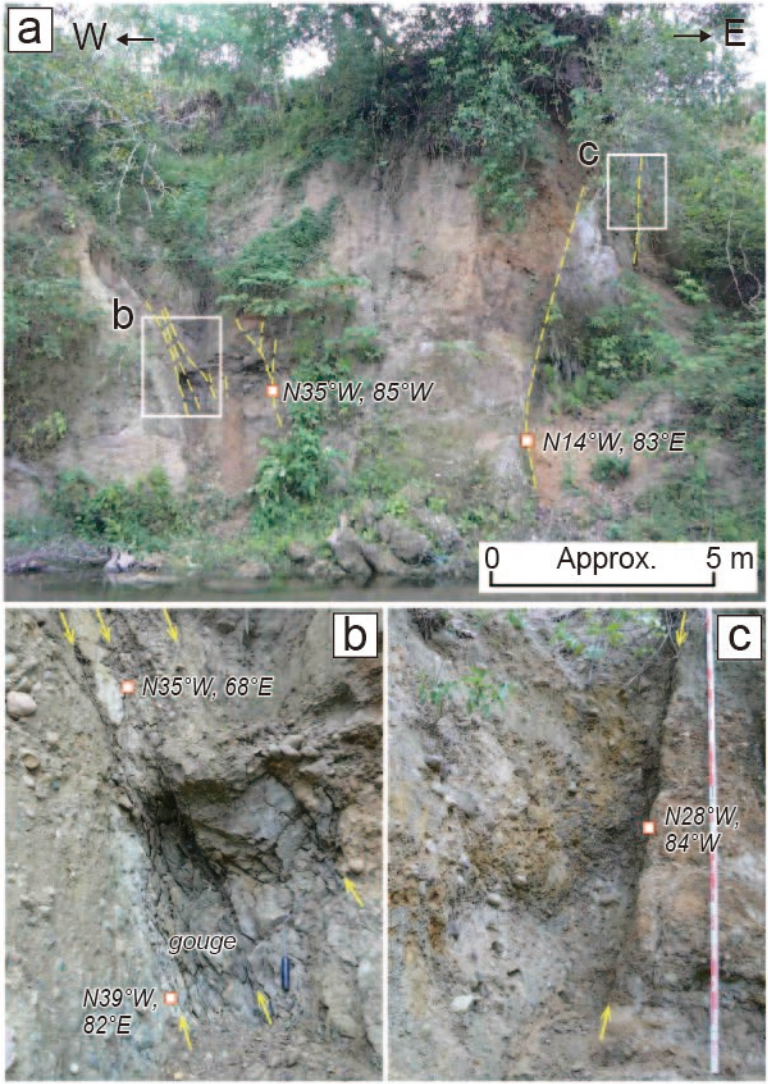
a
W
E
c
b
N35°W, 85°W
N14°W, 83°E
0
Approx.
5 m
b
N35°W, 68°E
gouge
N39°W,
82°E
c
N28°W,
84°W

Fig. 6

Figure 7.

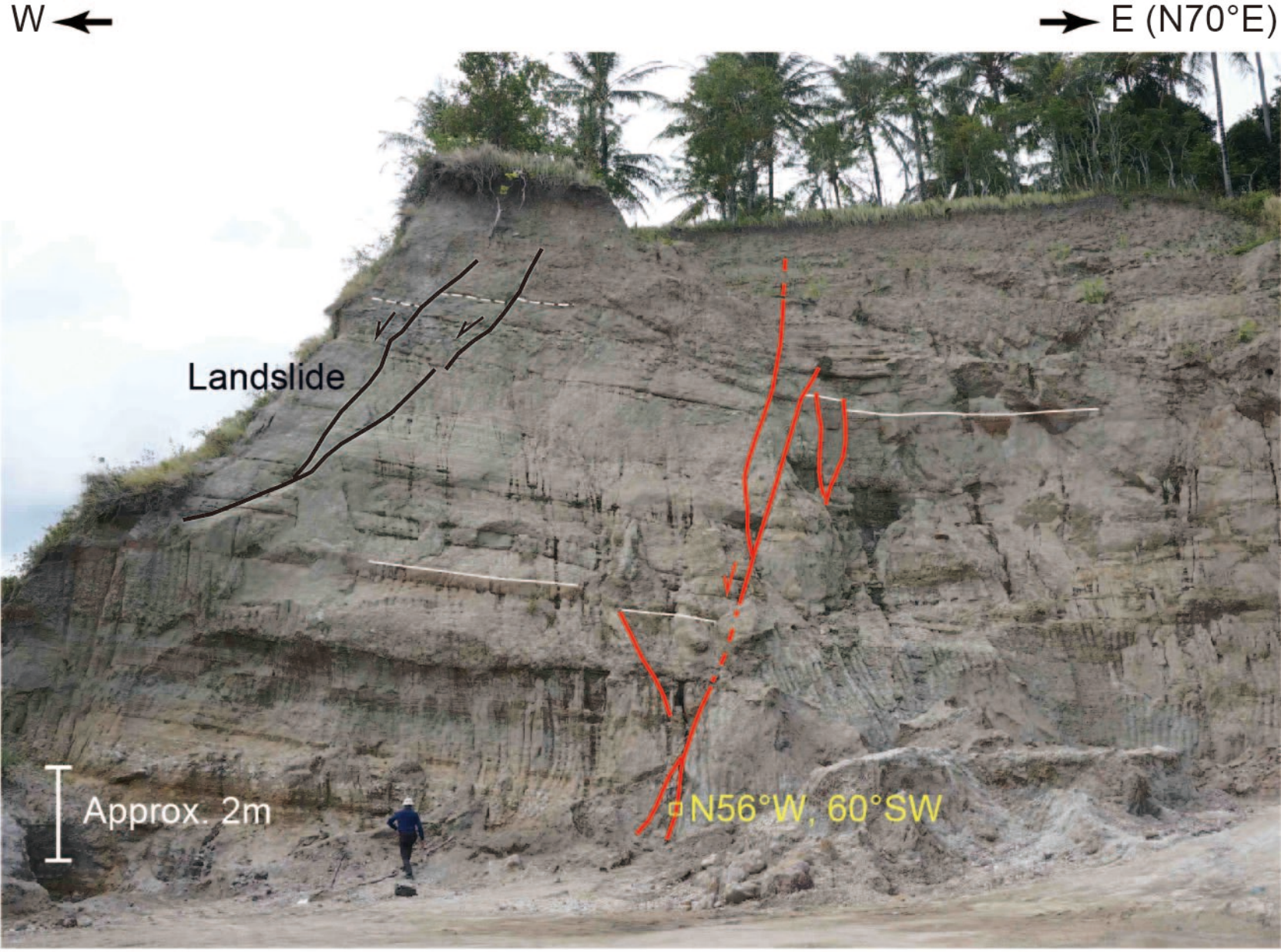

Fig. 7

Figure 8.

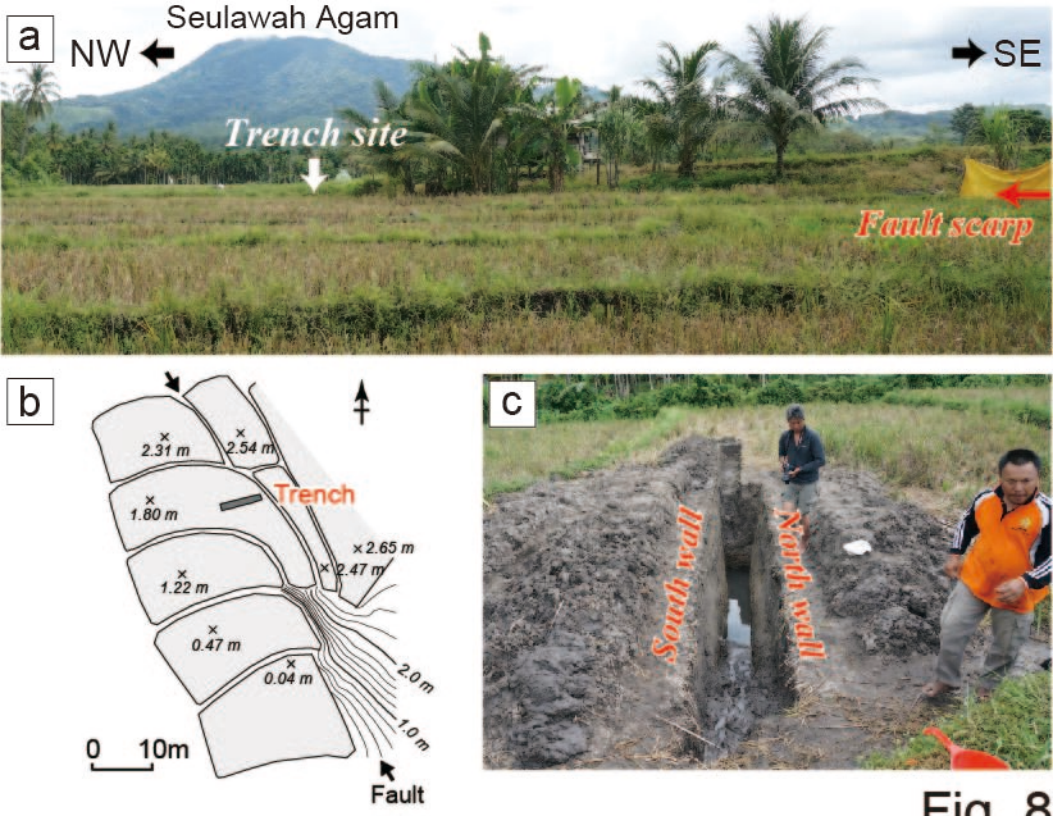
a
Seulawah Agam
NW
SE
Trench site
Fault scarp
b
2.31 m
2.54 m
1.80 m
Trench
2.65 m
2.47 m
1.22 m
0.47 m
0.04 m
2.0 m
1.0 m
0 10m
Fault
c
South wall
North wall

Fig. 8

Figure 9.

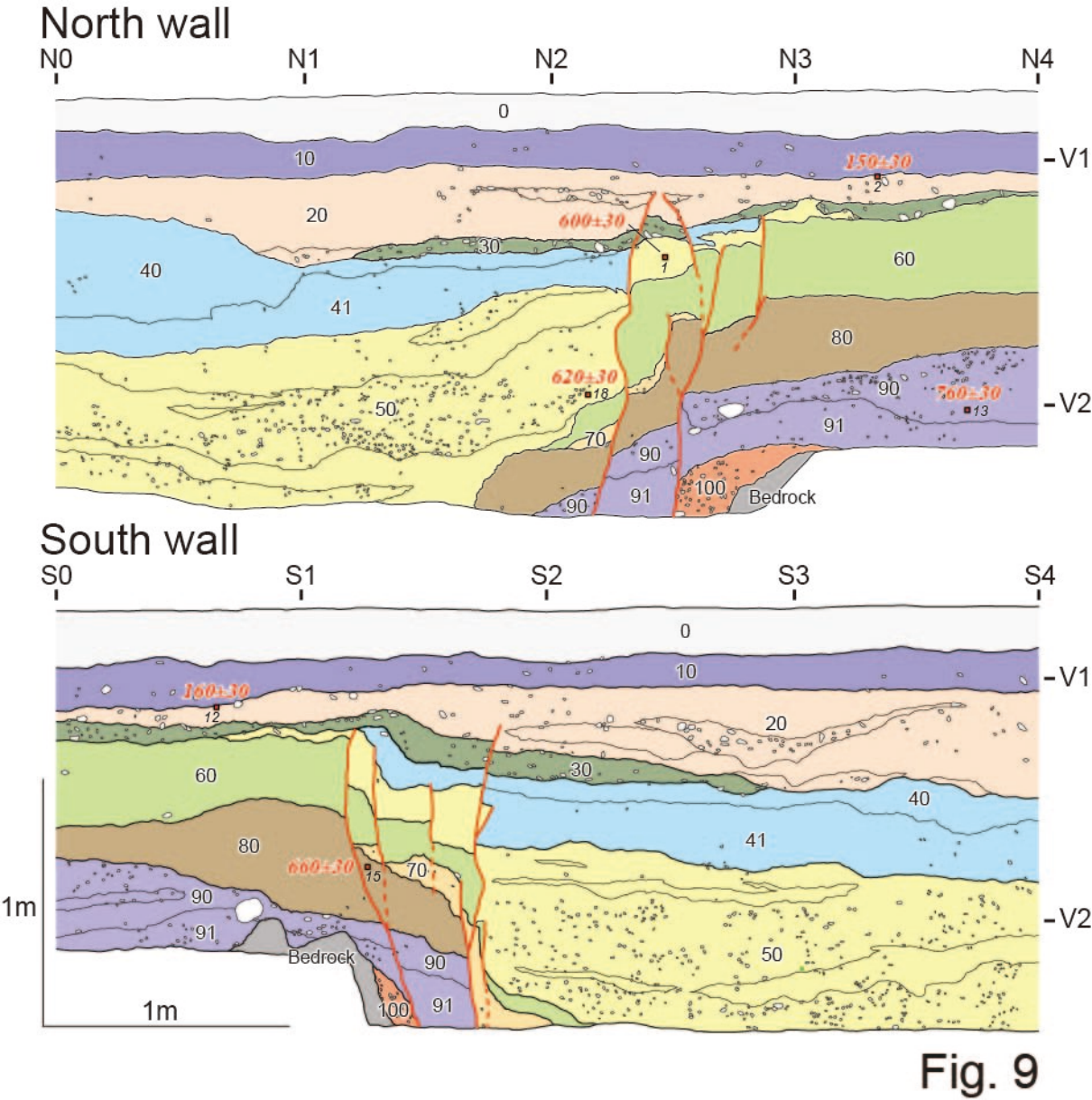
North wall
N0
N1
N2
N3
N4
0
10
20
30
40
41
50
60
70
80
90
91
100
Bedrock
150±30
2
600±30
1
620±30
18
760±30
13
V1
V2
South wall
S0
S1
S2
S3
S4
0
10
20
30
40
41
50
60
70
80
90
91
100
Bedrock
160±30
12
660±30
15
V1
V2
1m
1m

Fig. 9

Figure 10.

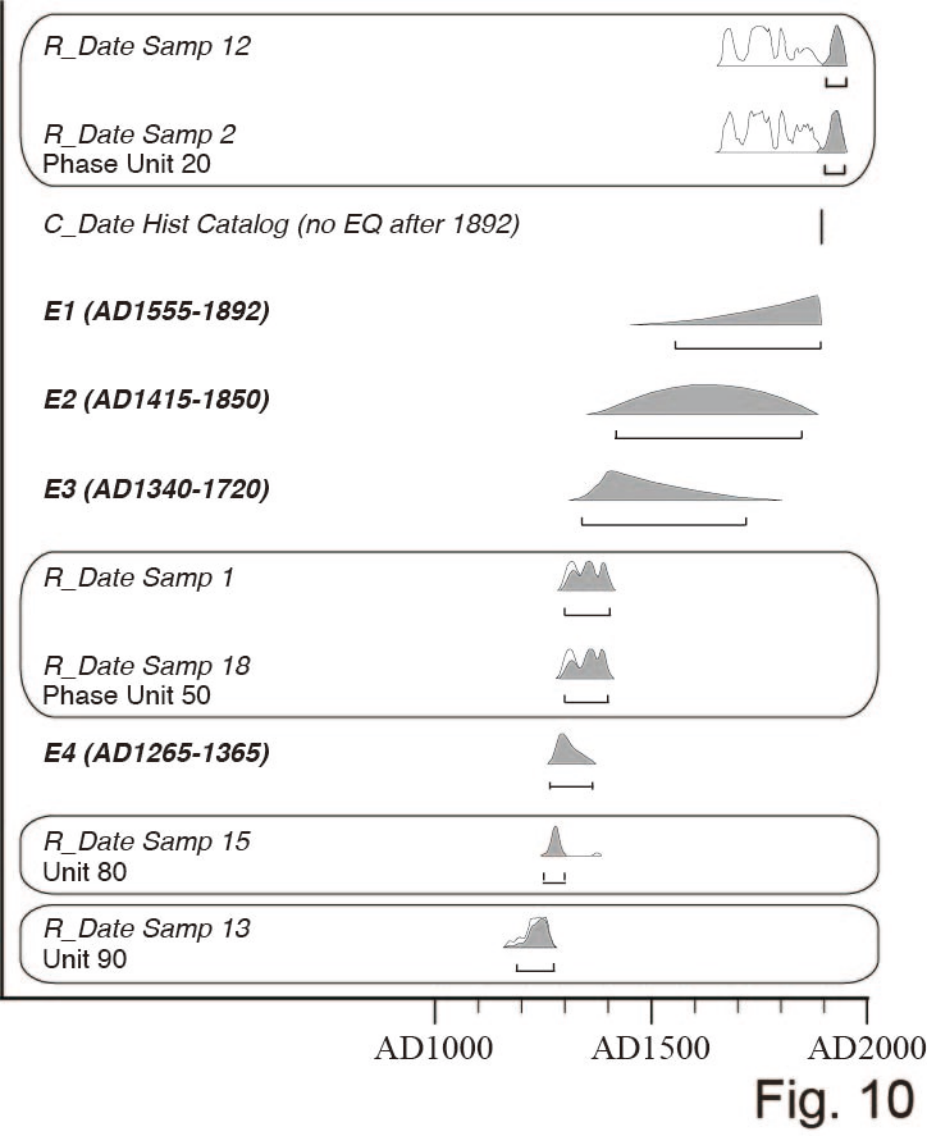
R_Date Samp 12
R_Date Samp 2
Phase Unit 20
C_Date Hist Catalog (no EQ after 1892)
E1 (AD1555-1892)
E2 (AD1415-1850)
E3 (AD1340-1720)
R_Date Samp 1
R_Date Samp 18
Phase Unit 50
E4 (AD1265-1365)
R_Date Samp 15
Unit 80
R_Date Samp 13
Unit 90
AD1000
AD1500
AD2000

Fig. 10

Strat. unit	Sample No.	Lab. No. (Beta-)	Material	Measured ^{14}C age (yBP)	$\delta^{13}C$ (‰)	Conventional ^{14}C age (yBP)	Calendar age (2σ)
20	2	414078	charred mat.	210±30	-28.8	150±30	AD1665-1785, 1795-1890, 1905-post 1950
20	12	417649	charred mat.	200±30	-27.6	160±30	AD1665-1710, 1720-1890, 1910-post 1950
50	1	414077	charred mat.	610±30	-25.9	600±30	AD1295-1410
50	18	417650	charred mat.	620±30	-24.7	620±30	AD1290-1405
80	15	405610	charred mat.	720±30	-28.8	660±30	AD 1280-1320, 1350-1390
90	13	414079	wood	810±30	-28.2	760±30	AD 1220-1285

Unit	Description
Unit 0	About 20 cm thick cultivated soil for rice farming. Numerous dry cracks developed after excavation.
Unit 10	Brownish and compact fine to medium sand. This unit contains sub-rounded to rounded pebbles as large as 4 cm in diameter. The topmost part of this unit includes abundant oxidized root traces. Numerous dry cracks developed down to this unit. This unit is interpreted as paleosol developed from unit 20.
Unit 20	Pale- to yellowish-brown fine sand. The boundary between this unit and the overlying unit 10 is gradual and irregular. A few layers of channel deposits with sub-rounded to rounded pebbles as large as 4 cm in diameter are identified on the north and south walls. Two charcoal samples obtained from this unit were dated at 150±30 yBP and 160±30 yBP.
Unit 30	Grayish-brown and matrix-supported deposits with sub-rounded to rounded pebbles as large as 4 cm in diameter. The unit is observed only on the eastern part of the trench walls.
Unit 40	Brown fine sand to silt containing a small number of pebbles less than 5 cm in diameter. This unit thins to the east and is distributed only within and west of the fault zone.
Unit 41	Yellowish-brown fine sand containing pebbles less than 1 cm in diameter. Fragments of spiral shells are scattered. The thickness of units 40 and 41 combined changes drastically across the fault zone.
Unit 50	Pale-yellow layer composed of pebbles and sands. Shell fragments are scattered throughout this unit. This unit contains sandstone granules less than 3 mm in diameter within and east of the fault zone. West of the fault zone, the unit is composed of a series of channel deposits composed of well-sorted, rounded pebbles less than 3 cm in diameter and medium sand with abundant charcoals and wood fragments. West of the fault zone, this unit eroded the underlying strata. Two charcoal samples obtained from this unit were darted at 600±30 yBP and 620±30 yBP.
Unit 60	Pale-brown silt. This unit is very homogenous without the inclusion of gravels. This unit is thicker on the east of the fault zone.
Unit 70	Pebbles observed only within and immediately west of the fault zone. This unit contains abundant fragments of shells.
Unit 80	Pale-yellow medium sand with lenses of coarse sand. This unit is not exposed on the south wall west of the fault zone. Charcoal obtained from this unit was dated at 660±30 yBP.
Unit 90	Matrix-supported gravel bed composed of rounded andesite clasts as large as 10 cm in diameter. The matrix is medium to coarse sand. A wood fragment obtained from this unit was dated at 760±30 yBP.
Unit 91	Brown fine sand with scattered shell fragments. The upper surface of this unit was eroded by the overlying unit 90.
Uni100	Matrix-supported sub-rounded to rounded sandstone pebbles as large as 3 cm in diameter. This unit contains